

MODELLING AND COUNTERACTING MICROBUNCHING INSTABILITY IN SPREADER LINES OF RADIOFREQUENCY AND PLASMA-BASED ACCELERATORS FOR FREE ELECTRON LASERS

G. Perosa^{*1}, S. Di Mitri¹, Università degli Studi di Trieste, Trieste, Italy
¹also at Elettra-Sincrotrone Trieste, Trieste, Italy

Abstract

High energy radiofrequency and plasma-driven accelerators target electron beam brightness suitable for x-ray free-electron lasers. Microbunching instability can be enhanced during beam transport through the spreader line from the accelerator to the undulator, degrading the brightness of the accelerated beam and therefore reducing the lasing efficiency. We present a semi-analytical model of the instability, benchmarked with experimental data at the FERMI free-electron laser, in the presence of intrabeam scattering and beam heating. Strategies for minimization of the instability both in conventional and plasma-based accelerators are discussed.

INTRODUCTION

Microbunching instability [1, 2] is one of the main reason behind spectral degradation of narrow bandwidth free electron lasers, preventing the extension of longitudinal coherence to the water window (from 300 to 500 eV) and higher photon energy. As the name suggests, this phenomenon is a cascade process that originates from density modulation of the charge distribution. Because of its broadband gain, it is able to capture and amplify modulations from several μm to few 100's of μm wavelength. Passing through dispersive regions, such as magnetic bunch length compressors, collimators and multi-bend transfer lines, emission of synchrotron radiation enhances the longitudinal modulations amplified along the beamline. The large amplitude μm -scale modulations in the final electron beam longitudinal phase space translate into large slice energy spread, causing the reduction of photon brilliance. Moreover, the mixing of MBI-frequencies and FEL coherent emission generates shot-to-shot fluctuations of the multilines FEL, leading to the appearance of sidebands at specific frequencies.

Although some differences between the transport of high-brightness beams driven by radiofrequency (RF) accelerators and the one driven by plasma accelerators can be pointed out, the two schemes are united by the employment of multi-bend switchyard lines downstream from the acceleration stage.

These sections, also called spreader lines, can become sources for MBI given the alternation of straight sections and dipoles. In the former ones, energy modulations are excited through longitudinal space charge (LSC), while in the latter the modulations are enhanced and converted back to density non-uniformities.

* giovanni.perosa@elettra.eu

MICROBUNCHING INSTABILITY IN SPREADER LINES

Semi-analytical Matrix Method

The beam spurious harmonic content can be described following the Bosch-Kleman (BK) [3] formalism which allows the description of MBI in linear regime along dispersive sections of arbitrary geometry, such as multi-bend transfer lines. The model introduces a 2-dimensional vector space of longitudinal modulations of electrons bunches. All the collective phenomena, namely longitudinal space-charge (LSC), coherent synchrotron radiation (CSR) and coherent edge radiation (CER), possibly including the effect of vacuum chamber shielding, are introduced by means of impedances $Z(\lambda)$ [4], as a function of the modulation wavelength λ . The contributions to beam modulations are expressed via matrix multiplication. Although we limit our discussion to LSC, CSR and CER, it is always possible to add piece-wise other longitudinal collective effects, as long as they can be described by impedances. This makes the model highly adaptable to any kind of section and to any degree of accuracy in the description of the beam line.

Given the integrated impedance $Z_{col}(\lambda)$ of a specific collective effect along a section of length L , the corresponding matrix acting on the modulations space is

$$S_L = \frac{1}{E(L)} \begin{pmatrix} E(L) & 0 \\ -Z_{col}(\lambda)I & E(0) \end{pmatrix}, \quad (1)$$

where $E(z)$ is the energy value along the section, with $0 < z < L$.

When the section is energy-dispersive, the effect of longitudinal Landau Damping can be included through the following matrix

$$\mathcal{D} = \begin{pmatrix} F(\lambda) & ik(\lambda)R_{56}F(\lambda) \\ iG(\lambda)/E & F(\lambda) - k(\lambda)R_{56}G(\lambda)/E \end{pmatrix}, \quad (2)$$

where R_{56} is the element of the transfer matrix that couples the longitudinal coordinates (z, δ) and the functions F and G are

$$F(\lambda) = \int \cos[k(\lambda)R_{56}\delta/E]f(\delta)d\delta \quad (3)$$

$$G(\lambda) = \int \sin[k(\lambda)R_{56}\delta/E]f(\delta)\delta d\delta, \quad (4)$$

in which $f(\delta)$ is the electrons energy distribution. These quantities embody the suppression of gain due to uncorrelated energy spread and they depend on the slice energy profile. More precisely, the dynamics of microbunching inside a dispersive region is regulated by the harmonic content of the slice energy distribution, i.e. by its Fourier transform.

Starting with a specific but arbitrary profile for $f(\delta)$ and associated energy spread $\sigma_E(0)$, this value will be increased after a L-long section by intrabeam scattering (IBS) [5, 6], resulting in an enlargement of the distribution width [7]. It is important to underline that, in our model, MBI and IBS are partially decoupled since scattering effects can be neglected for a threshold modulation wavelength well below the micro-scale [8]. This wavelength depends only on the geometry of the dispersive section and beam optics. A fully coupled treatment is modeled and solved numerically by other authors [9–11].

The whole spreader lines can be therefore described by a matrix T , given by [7]

$$T(\lambda) = \prod_i S_i(\lambda) * \mathcal{D}_i(\lambda), \quad (5)$$

where the index i runs over the number of dipoles.

We collapse the information of the microbunching instability “strength” into the spectral integral of the energy modulation curve in the aforementioned wavelength range, weighted by the instability gain. We refer to this quantity as σ_{MBI} , defined as

$$\sigma_{MBI}^2 = \frac{2ec}{I_0} \int \frac{|T_{21}(\lambda)|^2}{\lambda^2} d\lambda, \quad (6)$$

where $T_{21}(\lambda)$ is the entry of the overall transport matrix T .

Results

From the mathematical point of view, the differences between RF-driven and plasma-based accelerators translates in a different initial condition. In the former scheme, the beam reaches the spreader line after several phase space manipulations and after a path length that ranges from tens to thousands of meter, allowing the accumulation of energy modulations. In the latter scheme, the instability gain is basically limited to the spreader.

We apply our model to study the evolution of MBI for an electron beam parameters at the exit of a plasma accelerator, which are similar to those of the Eupraxia proposal [12, 13] (shown in Table 1) varying initial energy spread and spreader optics.

The semi-analytical estimation of the MBI through the switchyard indicates that the isochronous optics minimizes the instability with respect to both positive and negative momentum compaction. However, the isochronous optics blue shifts the maximum gain at sub- μm wavelengths, which could still interfere with lasing at < 1 nm. We, therefore, assess the effective suppression of the instability by calculating the final effective slice energy spread vs. the initial one (see Fig. 1). In doing so, we find that the optics associated with a larger gain, i.e., non-zero R_{56} , shows a non-linear trend of σ_{MBI} for $\sigma_{E,in} < 60$ keV, which is a signature of the phase space dominated by the instability. At larger values of $\sigma_{E,in}$, the dependence becomes linear, which reflects the preservation of the longitudinal emittance (Liouvillian behavior), i.e., the instability is largely mitigated or suppressed.

Table 1: Electron Beam and Switchyard Parameters at the Exit of the Plasma Accelerator

Parameter	Value
Energy	1 GeV
Charge	30 pC
Peak Current	3 kA
Duration, RMS	4 fs
Slice energy spread, RMS	10 keV - 100 keV
Normalized emittance, RMS	0.3 μrad
Transverse size, RMS	$< 40 \mu\text{m}$
Dipole length	0.5 m
Dipole bending angle	3.5 deg
Drift length	5 m
$ R_{56} $	< 3 mm
Average betatron function	10 m

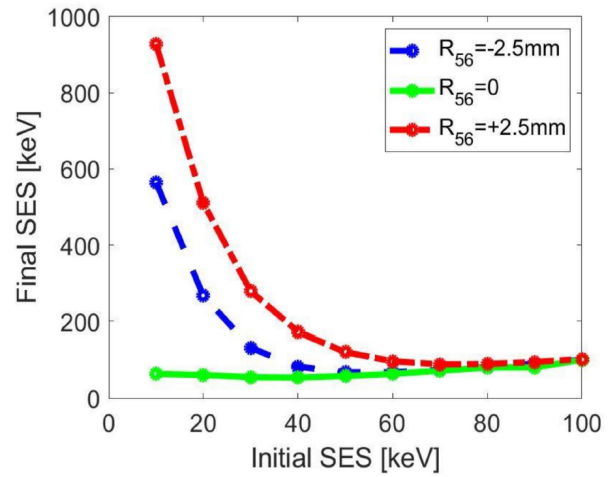


Figure 1: The calculated final slice energy spread, including the term σ_{MBI} vs. initial slice energy spread for three switchyard optics. Published in [13].

On the contrary, the isochronous optics shows σ_{MBI} as being almost independent from $\sigma_{E,in}$ for small values of this parameter (i.e., the non-linear dependence is strongly suppressed), while a linear dependence still exists for larger values.

The proposed model has been used also to shed light on the performance of echo-enabled harmonic generation (EEHG) scheme realized at FERMI [14]. The goal of the investigation was the improvement of the spectral brightness and mitigation of the FEL sideband instability by tuning the momentum compaction of a transfer line [15]. The EEHG spectrum and intensity was recorded for three values of the spreader momentum compaction, i.e., $R_{56} \cong -2, 0, +2$ mm.

In this case, the semi-analytical model takes into account the energy modulations excited during acceleration and the effect of the magnetic bunch length compressor. Our treatment suggests an interpretation, based on phase mixing [16], of the experimental results for the negative R_{56} , which exhibit a reduced sideband with respect to the other cases

(Fig. 2). When the beam reaches the spreader with a density modulation generated by the instability in the accelerator the longitudinal slippage of particles, generated by the nonzero R_{56} times the local energy chirp at the modulation scale, smoothens the beam longitudinal phase space. This translates into a redshift of the peak gain toward wavelengths that do not interference anymore with the FEL natural bandwidth. This picture is consistent with theoretical and numerical results reported also in Refs. [17, 18]. The MBI strength predicted by the model is shown in the inset of Fig. 3. Although the calculated σ_{MBI} cannot be directly related to the measured FEL spectral purity, the weaker the instability gain is, the lower the σ_{MBI} is, and the smaller the amount of FEL energy is expected to be dispersed into sidebands.

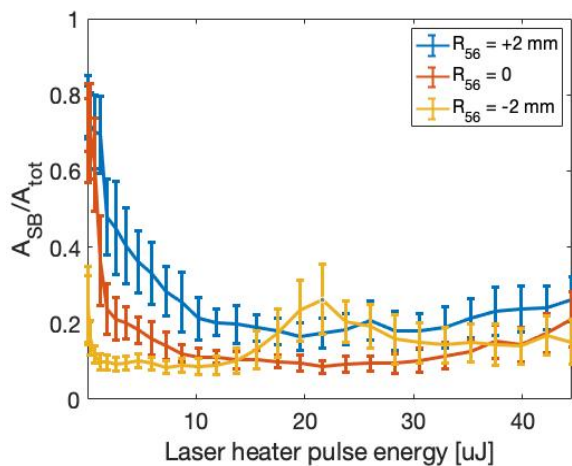


Figure 2: Ratio of the pedestal signal over the total FEL signal. Published in [15].

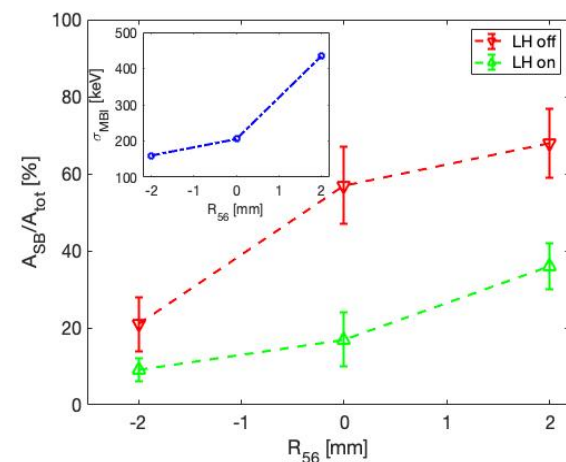


Figure 3: Measured average spectral area of sidebands with the laser heater turned off (red triangles) and on (green triangles). In the inset, predicted σ_{MBI} calculated for the laser heater off. Published in [15].

CONCLUSION

We present the results of a linear model of microbunching instability exploitable in dispersive region of arbitrary geometry, comparing it with experimental data. The implementation of this semi-analytical matrix model is a fast and comprehensive tool to design, predict and optimize microbunching instability along multi-bend transfer lines. Our study suggests that, in absence of strong initial modulations generated by the instability, the isochronous scheme is the most suitable for MBI reduction.

ACKNOWLEDGEMENT

The authors would like to thank E. M. Allaria, L. Badano, N. Bruchon, P. Cinquegrana, M. B. Danailov, A. Demidovich, G. De Ninno, L. Giannessi, N. Mirian, G. M. Penco, P. Rebernik, E. Roussel, P. Sigalotti, S. Spampinati, M. Veronese, M. Trovò for the support during the data collection, as in [15].

REFERENCES

- [1] E. L. Saldin, E. A. Schneidmiller, and M. Yurkov, “Klystron instability of a relativistic electron beam in a bunch compressor”, *Nucl. Instrum. Methods Phys. Res. A*, vol. 490, pp. 1-8, 2002. doi:10.1016/S0168-9002(02)00905-1
- [2] S. Di Mitri, “Coherent synchrotron radiation, and microbunching instability”, in *Proc. CERN Accelerator School: Free Electron Lasers and Energy Recovery Linacs (CAS'16)*, Hamburg, Germany, 2016. doi:10.23730/CYRSP-2018-001.381
- [3] R. A. Bosch, K. J. Kleman, and J. Wu, “Modeling two-stage bunch compression with wakefields: Macroscopic properties and microbunching instability”, *Phys. Rev. Spec. Top. Accel. Beams*, vol. 11, p. 090702, 2008. doi:10.1103/PhysRevSTAB.11.090702
- [4] B. W. Zotter and S. A. Kheifets, *Impedances and Wakes in High-Energy Particle Accelerators*. Hackensack, NJ, USA: World Scientific Pub. Co. Inc., 1998.
- [5] A. Piwinski, “Intra-beam scattering”, in *Proc. 9th Int. Conf. on High Energy Accelerators*, Stanford, CA, USA, May 1974, pp. 405-409. doi:10.5170/CERN-1992-001.226
- [6] J. Bjorken and S. Mtingwa, “Intrabeam scattering”, *Part. Accel.*, vol. 13, pp. 115-143, 1983. doi:0031-2460/83/1303/0115
- [7] S. Di Mitri *et al.*, “Experimental evidence of intrabeam scattering in a free-electron laser driver”, *New J. Phys.*, vol. 22, p. 083053, 2020. doi:10.1088/1367-2630/aba572
- [8] G. Perosa and S. Di Mitri, “Matrix model for collective phenomena in electron beam’s longitudinal phase space”, *Sci. Rep.*, vol. 11, p. 7895, 2021. doi:10.1038/s41598-021-87041-0
- [9] C. Y. Tsai *et al.*, “Theoretical formulation of phase space microbunching instability in the presence of intrabeam scattering for single-pass or recirculation accelerators”, *Phys. Rev. Accel. Beams*, vol. 23, p. 124401, 2020. doi:10.1103/PhysRevAccelBeams.23.124401

- [10] C. Y. Tsai and W. Qin, “Semi-analytical analysis of high-brightness microbunched beam dynamics with collective and intrabeam scattering effects”, *Phys. Plasma*, vol. 28, p. 013112, 2021. doi:10.1063/5.0038246
- [11] C. Y. Tsai and W. Qin, “Microbunching instability in the presence of intrabeam scattering for single-pass accelerators”, presented at the 12th Int. Particles Accelerators Conf. (IPAC’21), May 2021, paper THXA04, this conference.
- [12] EUPRAXIA Conceptual Design Report, <http://www.lnf.infn.it/sis/preprint/pdf/getfile.php?filename=INFN-18-03-LNF.pdf>
- [13] S. Di Mitri and G. Perosa, “Electron Beam Transport in Plasma-Accelerator-Driven Free-Electron Lasers in the Presence of Coherent Synchrotron Radiation and Microbunching Instability”, *Physics*, vol. 2, pp. 521–530, 2020. doi:10.3390/physics2040029
- [14] P. Rebernik *et al.*, “Coherent soft X-ray pulses from an echo-enabled harmonic generation free-electron laser”, *Nat. Photonics*, vol. 13, pp. 555-561, 2019. doi:10.1038/s41566-019-0427-1
- [15] G. Perosa *et al.*, “Linear optics control of sideband instability for improved free-electron laser spectral brightness”, *Phys. Rev. Accel. Beams*, vol. 23, p. 110703, 2020. doi:10.1103/PhysRevAccelBeams.22.080702
- [16] S. Di Mitri and S. Spampinati, “Microbunching Instability Suppression via Electron-Magnetic-Phase Mixing”, *Phys. Rev. Lett.*, vol. 112, p. 134802, 2014. doi:10.1103/PhysRevLett.112.134802
- [17] M. Venturini and J. Qiang, “Transverse space-charge induced microbunching instability in high-brightness electron bunches”, *Phys. Rev. Accel. Beams*, vol. 18, p. 054401, 2015. doi:10.1103/PhysRevSTAB.18.054401
- [18] K. Zhang, L. Zeng, Z. Qi, C. Feng, and D. Wang, “Eliminating the microbunching-instability-induced sideband instability in a soft x-ray self-seeding free-electron laser”, *Nucl. Instrum. Methods Phys. Res., Sect. A*, vol. 882, pp. 22-29, 2018. doi:10.1016/j.nima.2017.10.060